Molecular structure and bonding character of mono and divalent metal cations (Li+, Na+, K+, Be2+, Mg2+, and Ca2+) with substituted benzene derivatives: AIM, NBO, and NMR analyses

4 AUTHORS, INCLUDING:

Fariba Mollania
University of Birjand
24 PUBLICATIONS **101** CITATIONS

SEE PROFILE

ORIGINAL RESEARCH

Molecular structure and bonding character of mono and divalent metal cations (Li$^+$, Na$^+$, K$^+$, Be^{2+}, Mg^{2+}, and Ca^{2+}) with substituted benzene derivatives: AIM, NBO, and NMR analyses

Azadeh Khanmohammadi · Heidar Raissi · Fariba Mollania · Lila Hokmabadi

Abstract Cation–π complexes between several cations (Li$^+$, Na$^+$, K$^+$, Be^{2+}, Mg^{2+}, and Ca^{2+}) and different π-systems such as para-substituted (F, Cl, OH, SH, CH$_3$, and NH$_2$) benzene derivatives have been investigated by UB3LYP method using 6-311++G** basis set in the gas phase and the water solution. The ions have shown cation–π interaction with the aromatic motifs. Vibrational frequencies and physical properties such as dipole moment, chemical potential, and chemical hardness of these compounds have been systematically explored. The natural bond orbital analysis and the Bader's quantum theory of atoms in molecules are also used to elucidate the interaction characteristics of the investigated complexes. The aromaticity is measured using several well-established indices of aromaticity such as NICS, HOMA, PDI, FLU, and FLUπ. The MEP is given the visual representation of the chemically active sites and comparative reactivity of atoms. Furthermore, the effects of interactions on NMR data have been used to more investigation of the studied compounds.

Keywords Cation–π interaction energy · Aromaticity indices · Charge transfer · Coupling constant · AIM and NBO

A. Khanmohammadi (✉) · L. Hokmabadi
Chemistry Department, Payame noor University, Mashad, Iran
e-mail: azadehkhanmohammadi@gmail.com

H. Raissi · F. Mollania
Chemistry Department, University of Birjand, Birjand, Iran

Introduction

The noncovalent interactions are important in biological and in artificial supramolecular structures, including ion pairing, hydrogen bonding, halogen bonding, cation–π, π–π interactions, etc. [1–12]. Among them, the interactions involving aromatic rings have attracted considerable attention, since they are extremely important binding forces in both chemical [2–4] and biological systems [5–7], such as protein folding [8, 9], the DNA double helix [10], enzyme–substrate complexes [11], and many supramolecular assemblies with artificial hosts [12].

The cation–π interaction is a noncovalent molecular interaction between the face of an electron-rich π system (e.g., benzene, ethylene, and acetylene) and an adjacent cation (e.g., Li$^+$ and Na$^+$). It is an example of noncovalent bonding between a monopole (cation) and a quadrupole (π system). The most studied cation–π interactions involve binding between an aromatic π system and an alkali-metal cation. These studies have shown that electrostatics dominates interactions in simple systems, and relative binding energies correlate well with electrostatic potential energy [13, 14]. Since cation–π interactions are predicted by electrostatics, it follows that cations with larger charge density interact more strongly with π systems. Several criteria influence the strength of the bonding: the nature of the cation, solvation effects, the nature of the π system, and the geometry of the interaction. In 2008, Dinadayalane et al. [15] focus on the interactions of alkali-metal cations (Li$^+$, Na$^+$, and K$^+$) with the cup-shaped molecules, tris(bicyclo[2.2.1]hepteno)benzene, and tris(7-azabicyclo[2.2.1]hepteno) benzene using ab initio methods. The obtained results showed that binding affinity of metal ion with the ligands under the study follows the order: Li$^+$> Na$^+$> K$^+$. Also, they demonstrated, using DFT

method, the binding of Li^+, Na^+, and K^+ with the benzene ring is enhanced by sequential annelation of six-membered aromatic ring or highly strained bicyclo[2.1.1]hexane ring [16]. The electronic properties of the substituents also influence the strength of the attraction [17]. The origin of substituent effects in cation–π interactions has often been attributed to polarization from electron donation or withdrawal into or out of the π system [18]. Recent computational work by Wheeler and Houk [19] strongly indicates that this effect is primarily due to direct through-space interaction between the cation and the substituent dipole. Sastry and co-workers [20–22] have provided new insights on cooperativity of cation–π and π–π interactions using quantum chemical calculations. Hassan and co-workers [23, 24] showed a significant increase of the strength of cation–π interactions by the presence of alkali-metal ions (Li^+, Na^+, and K^+), and the binding strength of cations with any given ligand follows the classical electrostatic trend: $Li^+ > Na^+ > K^+$. The present study is directed to investigate the cations (Li^+, Na^+, K^+, Be^{2+}, Mg^{+2}, and Ca^{+2}) interactions with different π-systems such as benzene (A), 1,4-difluorobenzene (B), 1,4-dichlorobenzene (C), hydroquinone (D), benzene-1,4-dithiol (E), *p*-xylene (F), and benzene-1,4-diamine (G). The main objective of this article is not only to determine the effects of cation–π interactions on the geometrical parameters, the binding strength, and topological properties of benzene ring with electron-donating (or withdrawing) substituents of the complexes formed, but also to gain further insight into the effect of mentioned interactions on NMR data. All ions are located along the main symmetry axis ($C_{2}v$) in the selected structures. Furthermore, in order to deal with this topic in depth, in the present work, we perform a comprehensive analysis of the change in aromaticity of aromatic rings upon complexation with a cation.

Theoretical methods

All calculations have been performed with Gaussian 03 program [25]. These complexes and their monomers have been optimized at the UB3LYP/6-311++G** level in the gas phase and solution. The solvent effect is performed for the water solution, using the polarizable continuum model (PCM) [26]. The binding energies are corrected for the basis set superposition error by the Boys–Bernardi counterpoise technique [27]. The procedure for obtaining the interaction energy is as follows:

$$\Delta E = E_{cation-\pi} - \left(E_{cation} + E_{\pi-system} \right)$$

The vibrational frequencies are calculated at the UB3LYP/6-311++G** level on the optimized geometries. Frequency calculations indicate that these complexes are

true minima. The topological electron charge density is analyzed by the atoms in molecules (AIMs) method [28], using the AIM2000 program [29] on the obtained wave functions at the UB3LYP/6-311++G** level. Also, the population analysis has been performed by the natural bond orbital (NBO) method [30] on the optimized structures using NBO program [31] under Gaussian 03 program package. The contour plot for visualization of the NBO result was constructed on NBOView (Version1.1) [32] software package using the standard keywords implemented therein. Furthermore, absolute NMR shielding values [33] are calculated using the Gauge-Independent Atomic Orbital (GIAO) method [34]. Herein, some spin–spin coupling constants ($^1J_{C–C}$, $^1J_{C–R'}$ and $^1J_{C–H}$) and the values of the proton shielding tensors have specifically been considered. The isotropic shielding values, $\sigma_{iso} = \frac{1}{3}(\sigma_{11} + \sigma_{22} + \sigma_{33})$ (σ_{ii} being the principal tensor components), are used to calculate the isotropic chemical shift δ with respect to TMS, $\delta_{iso}^{TMS} = (\sigma_{iso}^{TMS} - \sigma_{iso}^{X})$.

On the other hand, the aromaticity of the benzene complexes and its derivatives is measured using several well-established indices of aromaticity such as the nucleus-independent chemical shift (NICS) [35], the harmonic oscillator model of aromaticity (HOMA) [36], the para-delocalization index (PDI) [37], and the aromatic fluctuation index (FLU) [38]. In the present work, the R_{opt}, α, and δ_{ref} parameters for evaluation of HOMA and FLU indices are calculated at the UB3LYP/6-311++G** level of theory (for CC bond: $R_{opt,CC} = 1.396$ Å, $\alpha_{CC} = 88.54$, and $\delta_{ref\ CC} = 5.45$).

Results and discussions

The complexes are named according to the position of the substitutions (R) on the benzene ring (see Fig. 1). The

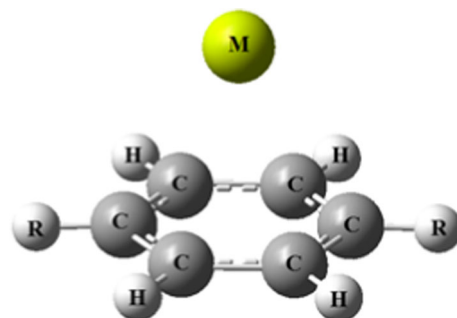**Fig. 1** The investigated complexes: The complexes of ion…para-substituted (H, F, Cl, OH, SH, CH_3 and NH_2) benzene derivatives. **M** = Li^+, Na^+, K^+, Be^{2+}, Mg^{2+} and Ca^{2+}, **R:** H = benzene (A), F = 1,4-difluorobenzene (B), Cl = 1,4 dichlorobenzene (C), OH = hydroquinone (D), SH = benzene-1,4-dithiol (E), CH_3 = *p*-xylene (F), and NH_2 = benzene-1,4-diamine (G)

calculations suggest that the size of cation and the nature of π-system are two influential factors that affect the nature of interaction. In the current investigation, the interactions are classified into two different types. Theoretical evidences have been used to demonstrate different natures for the interaction of π-systems with the alkali-metal cations and the alkaline-earth cations.

Molecular geometry and Binding energies

Table 1 presents the geometrical parameters and the values of complexation energy ($\Delta E_{ion-\pi}$) for cations (Li^+, Na^+, K^+, Be^{2+}, Mg^{2+}, and Ca^{2+}) with different π-systems such as para-substituted (F, Cl, OH, SH, CH_3, and NH_2) benzene derivatives. For each ligand, Be^{2+} binds much stronger than other divalent cations, while Li^+ interaction is the strongest among the monovalent cations. This trend follows the $d_{ion-\pi}$ distances corresponding to the complexes involving divalent and monovalent cations. As the ionic radius increases from Be^{2+} to Ca^{2+}, the interaction energy for cation–π complexes decreases; the same situation is observed in case of alkali-metal ion complexes. As shown in Table 1, the strength of interaction decreases in the following order: $Be^{2+} > Mg^{2+} > Ca^{2+} > Li^+ > Na^+ > K^+$ for any given aromatic ligand. The interaction energy data suggest that the nature of divalent cation complexation with ligands could be different from monovalent ones, and the forces other than electrostatics may play vital role in stabilizing these complexes. The electronic properties of the substituents also influence the strength of the attraction [17]. F, Cl, OH, and SH substitutions are σ-acceptors, whereas CH_3 and NH_2 act as σ, π-donors. In the studied complexes, the electrostatic (inductive and resonance) effects of substitutions influence the binding energies in opposite fashion. The comparison of complexation energies indicates that predominant factor in the NH_2-substituted ring is resonance (in comparison with induction). On the other hand, the F is an electronegative atom with induction predominate resonance and, therefore, the complex is destabilized by F electron-withdrawing substituent. Thus, as can be seen in Table 1, the electron-withdrawing groups such as F and Cl weaken the cation–π interaction, while the electron-donating substituents (CH_3 and NH_2) strengthen it. For each ion group (alkali metal and alkaline earth), the dependence between $|\Delta E_{ion-\pi}|$ and $d_{ion-\pi}$ (the distance between the ion and the center of aromatic ring) should separately be considered. Theoretical results show that the $d_{ion-\pi}$ decrease is accompanied by the $|\Delta E_{ion-\pi}|$ increase in each group. The geometrical parameters (see Table 1) indicate that Li^+ cation establishes shorter bond with the benzene ring than Na^+ and K^+ cations. This fact depends essentially on the size of the metal ion, because these interactions decrease with increase in the size of the

alkali-metal cation for all complexes. Furthermore, the nature of the interactions seems to be very similar for these three cations. This behavior is obvious for alkali-metal cations, because they belong to the same group of periodic Table. Based on our theoretical results, the $d_{ion-\pi}$ increase with the atomic number and the size of the alkali metals and also Li^+ binds more strongly than Na^+ and K^+. Because these complexes are largely electrostatic in nature, this is easily understood on the basis of the size or the charge density on metal cation. The greater charge density of the smaller metal cation leads to the greater strength of cation–π interaction in system. The K^+ cation creates the largest metal–benzene distance ($d_{ion-\pi}$) in comparison with the other ions, because of the longest ionic radius in this cation. Similar results have been obtained for alkaline-earth metal cations complexes too.

Furthermore, the geometrical parameters of the investigated complexes change in the presence of ion–π interactions. Our theoretical results confirm that the increase in the C=C ($d_{C=C}$) and C–H (d_{C-H}) bond lengths and also the decrease in the C–R′ bond length ($d_{C-R'}$) are accompanied with increasing the $|\Delta E_{ion-\pi}|$ values (see Table 1). For instance, a comparison of bond lengths in the NH_2-substituted complex and its monomer (G) demonstrates significant changes during the complexation. In the case of G-Be^{2+} complex, the C–N bond length becomes shorter than the other ones ($\Delta d_{C-N} = -0.082$ Å, Δd is difference between bond lengths in the complex and its monomer). The presence of the Be^{2+} cation polarizes the C–N bond in such a way that N atom transfers a certain amount of electron density; as a result, in comparison with the other complex, the C–C bond becomes longer ($\Delta d_{C-C} = 0.042$ Å). Also, the C–N bond shortens because the electron-donating N atom tends to compensate the electron deficiency on the rings.

The natural charges (the nuclear charge minus the summed natural populations of natural atomic orbitals on the atom) on the H and R′ atoms (q_H and $q_{R'}$) are also given in Table 1. As it is obvious from this Table, the cation–π interaction increases q_H values, while decreases $|q_{R'}|$ amounts. The maximum $|\Delta E_{ion-\pi}|$ value corresponds to the highest charge transfer (Δq) upon complexation. In all of the complexes, the computed binding strength varies with changing the ratio of charge to-radius for cations. Indeed, the increment in this ratio is accompanied with increase in the electrostatic interaction between metal ion and active sites in the benzene ring, and also, charge transfer from active sites to metal ion enhances too. Inspection of our theoretical results reveals clearly that the cations act as electron-accepting centers, and π-electrons of the para-substituted benzene rings act as the electron-donating ones.

Another index closely related to the strength of the complexation energy is the shifting of the cation-π stretching frequencies. In order to better elucidate the

Table 1 The geometrical parameters (bond lengths (d) is in Å), natural atomic charges (e), complexation energies (kJ mol^{-1}), and topological properties of electron density (in au) calculated at the UB3LYP/6-311++G** level

Complex	d_{C-C}	d_{C-H}	$d_{C-R'}$	$d_{ion-\pi}$	q_H	$q_{R'}^{a}$	Δq	$\Delta E_{ion-\pi}$	ρ_{BCP}	$\nabla^2\rho_{BCP}$	ρ_{C-C}	ρ_{C-H}	$\rho_{C-R'}$	ρ_H	$\rho_{R'}$
A-Li$^+$	1.403	1.084	1.084	1.843	0.223	0.223	0.068	−150.69	0.0172	0.0908	0.3043	0.2851	0.2851	0.9076	0.9086
A-Na$^+$	1.401	1.084	1.084	2.407	0.210	0.210	0.055	−93.16	0.0105	0.0489	0.3051	0.2839	0.2839	0.9251	0.9222
A-K$^+$	1.399	1.084	1.084	2.892	0.203	0.203	0.048	−63.78	0.0085	0.0319	0.3062	0.2833	0.2833	0.9371	0.9378
A-Be^{2+}	1.420	1.087	1.087	1.295	0.315	0.315	0.160	−946.67	0.0558	0.1781	0.2946	0.2867	0.2868	0.7915	0.7929
A-Mg^{2+}	1.415	1.086	1.086	1.946	0.294	0.294	0.139	−485.29	0.0262	0.1109	0.2980	0.2862	0.2862	0.8338	0.8306
A-Ca^{2+}	1.408	1.086	1.086	2.372	0.270	0.269	0.115	−327.96	0.0219	0.0738	0.3021	0.2853	0.2853	0.8495	0.8510
B-Li$^+$	1.397	1.084	1.333	1.820	0.276	−0.089	0.072	−101.28	0.0157	0.0795	0.3109	0.2841	0.2682	0.8709	9.5918
B-Na$^+$	1.394	1.084	1.340	2.491	0.262	−0.103	0.058	−54.98	0.0092	0.0417	0.3123	0.2833	0.2622	0.8885	9.5974
B-K$^+$	1.392	1.084	1.344	2.970	0.253	−0.115	0.049	−33.97	0.0071	0.0266	0.3136	0.2829	0.2587	0.8999	9.6066
B-Be^{2+}	1.420	1.089	1.293	1.262	0.357	0.021	0.153	−836.08	0.0556	0.1717	0.2995	0.2835	0.3018	0.7634	9.5385
B-Mg^{2+}	1.413	1.087	1.309	1.994	0.349	−0.029	0.145	−395.23	0.0255	0.1025	0.3030	0.2839	0.2880	0.8040	9.5578
B-Ca^{2+}	1.405	1.087	1.320	2.412	0.316	−0.035	0.112	−253.77	0.0207	0.0677	0.3074	0.2834	0.2796	0.8290	9.5723
C-Li$^+$	1.403	1.083	1.733	1.883	0.259	0.535	0.079	−110.26	0.0164	0.0839	0.3043	0.2852	0.2047	0.8855	17.0820
C-Na$^+$	1.400	1.083	1.740	2.461	0.239	0.513	0.059	−61.92	0.0096	0.0437	0.3059	0.2845	0.2011	0.8983	17.1091
C-K$^+$	1.398	1.083	1.745	2.961	0.226	0.488	0.046	−39.83	0.0075	0.0285	0.3073	0.2841	0.1989	0.9124	17.1305
C-Be^{2+}	1.429	1.087	1.692	1.274	0.319	0.886	0.139	−895.05	0.0580	0.1848	0.2913	0.2856	0.2242	0.7869	16.8780
C-Mg^{2+}	1.421	1.086	1.708	1.958	0.309	0.783	0.129	−435.06	0.0270	0.1126	0.2954	0.2854	0.2166	0.8229	16.9502
C-Ca^{2+}	1.412	1.086	1.721	2.368	0.296	0.620	0.116	−286.36	0.0220	0.0745	0.3003	0.2848	0.2109	0.8479	17.0026
D-Li$^+$	1.405	1.084	1.351	1.847	0.231	−0.170	0.028	−151.63	0.0178	0.0934	0.3031	0.2817	0.2969	0.9177	9.0589
D-Na$^+$	1.402	1.084	1.359	2.412	0.216	−0.195	0.013	−93.54	0.0108	0.0498	0.3046	0.2806	0.2909	0.9309	9.0638
D-K$^+$	1.400	1.084	1.363	2.883	0.204	−0.207	0.001	−65.48	0.0089	0.0332	0.3062	0.2800	0.2875	0.9481	9.0671
D-Be^{2+}	1.431	1.087	1.306	1.331	0.320	−0.075	0.117	−991.22	0.0594	0.1954	0.2908	0.2838	0.3308	0.8133	9.0416
D-Mg^{2+}	1.423	1.086	1.324	1.956	0.308	−0.133	0.105	−512.94	0.0281	0.1190	0.2941	0.2831	0.3173	0.8512	9.0475
D-Ca^{2+}	1.414	1.086	1.336	2.357	0.275	−0.148	0.072	−352.45	0.0234	0.0804	0.2990	0.2821	0.3083	0.8762	9.0586
E-Li$^+$	1.411	1.085	1.772	1.840	0.244	−0.335	0.063	−146.39	0.0178	0.0936	0.2979	0.2840	0.1933	0.9193	15.7230
E-Na$^+$	1.407	1.085	1.778	2.400	0.229	−0.382	0.048	−89.84	0.0109	0.0504	0.2995	0.2830	0.1915	0.9346	15.7633
E-K$^+$	1.405	1.085	1.781	2.874	0.214	−0.406	0.033	−63.02	0.0087	0.0331	0.3012	0.2825	0.1907	0.9444	15.7679
E-Be^{2+}	1.438	1.087	1.736	1.305	0.314	−0.165	0.133	−1007.40	0.0609	0.2032	0.2843	0.2860	0.2033	0.8176	15.5311
E-Mg^{2+}	1.430	1.086	1.750	1.937	0.304	−0.243	0.123	−521.94	0.0289	0.1237	0.2884	0.2850	0.1994	0.8602	15.6086
E-Ca^{2+}	1.420	1.087	1.764	2.318	0.278	−0.257	0.097	−361.56	0.0238	0.0818	0.2934	0.2841	0.1957	0.8842	15.6538
F-Li$^+$	1.408	1.085	1.507	1.810	0.255	−0.554	0.110	−172.94	0.0187	0.1001	0.3017	0.2837	0.2500	0.9240	5.9782
F–Na$^+$	1.406	1.085	1.509	2.371	0.236	−0.583	0.091	−107.77	0.0115	0.0543	0.3028	0.2824	0.2495	0.9411	5.9751
F-K$^+$	1.400	1.086	1.509	2.818	0.216	−0.572	0.090	−74.51	0.0094	0.0356	0.3041	0.2724	0.2493	0.9426	5.9592
F-Be^{2+}	1.430	1.086	1.497	1.203	0.322	−0.523	0.177	−1045.50	0.0594	0.1992	0.2906	0.2864	0.2505	0.8173	5.9794
F-Mg^{2+}	1.424	1.086	1.501	1.916	0.318	−0.492	0.173	−553.99	0.0285	0.1261	0.2940	0.2852	0.2504	0.8549	5.9836
F-Ca^{2+}	1.415	1.087	1.504	2.335	0.297	−0.553	0.152	−382.63	0.0241	0.0822	0.2986	0.2841	0.2499	0.8824	5.9809
G-Li$^+$	1.413	1.085	1.381	1.813	0.211	−0.264	0.071	−197.54	0.0190	0.1022	0.2990	0.2821	0.3085	0.9304	8.0553
G-Na$^+$	1.409	1.085	1.392	2.365	0.199	−0.282	0.059	−131.72	0.0118	0.0557	0.3009	0.2809	0.3023	0.9440	8.0346
G-K$^+$	1.406	1.085	1.397	2.813	0.186	−0.284	0.046	−99.10	0.0100	0.0382	0.3025	0.2803	0.2990	0.9537	8.0335
G-Be^{2+}	1.442	1.086	1.327	1.351	0.302	−0.235	0.162	−1,129.60	0.0624	0.2164	0.2856	0.2841	0.3427	0.8338	8.0860
G-Mg^{2+}	1.433	1.086	1.345	1.942	0.288	−0.312	0.148	−620.45	0.0301	0.1318	0.2893	0.2834	0.3300	0.8682	8.0745
G-Ca^{2+}	1.423	1.086	1.364	2.316	0.254	−0.293	0.114	−444.16	0.0255	0.0889	0.2944	0.2825	0.3196	0.8912	8.0660

[a] R' = H, F, Cl, O, S, C, N atoms in R substitution of A, B, C, D, E, F, and G complexes, respectively

strength of these interactions, vibrational frequencies for all of complexes are calculated. It is well established that the stronger the complexation energy, the larger is this shifting. Table 2 presents the stretching frequencies (v) of the cation–π contact (interaction) for the investigated complexes. It is important to emphasize that with strengthening of cation–π interactions, its stretching frequencies shift to upper wavenumbers (see Table 2). Our calculations indicate that the Be^{2+}-π stretching frequency for the B complex appears blue shifted by ca. 59 cm^{-1} with respect to A complex, whereas the K$^+$-π stretching frequency for the B complex appears red shifted by ca. 31 cm^{-1}. The maximum and minimum of stretching frequencies correspond to the complexes with Be^{2+} and K$^+$ ions, respectively.

Considering the results tabulated in Table 2, with only a few exceptions, upon substitution in R position (see Fig. 1), the cation-π stretching frequencies shift to upper wavenumbers with respect to the unsubstituted complex (A); as a result, performing such comparison confirms that the cation–π interaction enhances during complexation. Furthermore, according to our theoretical results on the Be^{2+} complexes, the greatest shifts observe for the electron-withdrawing substitutions (except for E-Be^{2+}), while the smallest shifts correspond to the electron-donating ones (except for G-Be^{2+}). Also, the stretching frequency shifts of the K^+ complexes increase by the electron-withdrawing substituents (except for C-K^+), but the reverse is true for the electron-donating substituents. Selected vibrational frequencies for the different π-systems and complexes are listed in Table 2. We discuss the changes in the selected vibrational frequencies caused by different metal ions complexed with the different π-systems. The out-of-plane bending vibrations of aromatic C–H bonds appear in the region of 700–950 cm^{-1}. Indeed, the out-of-plane C–H bending frequencies of the π systems are blue shifted upon complexation of metal ions with the different π-systems. The Li^+ gives the highest blue shift followed by Na^+ and K^+. A similar trend is observed for divalent cations. Also, our theoretical results are in agreement with outcomes of Dinadayalane et al. [15, 16]. The correlation matrices for the correlations among v, $\Delta E_{ion-\pi}$, ρ_{BCP}, $\nabla^2\rho_{BCP}$, G, and $d_{ion-\pi}$ properties have been reported in Table 3. Among mentioned matrices, ν shows the best linear relationship with $\Delta E_{ion-\pi}$, ρ_{BCP}, $\nabla^2\rho_{BCP}$, G, and $d_{ion-\pi}$ properties, with good correlation coefficients (greater than 0.8). It is found that the interactions strength is controlled predominately by stretching vibrational frequencies. In this case, the increase of the stretching vibrational frequency value is associated with the strengthening of the donor–acceptor interaction.

AIM analysis

The calculated topological parameters of these complexes are given in Table 1. The calculated topological parameters of these complexes are given in Table 1. The calculated electron density properties show that the cation–π interactions have low ρ (ranging from 0.0071 to 0.0624) and are also characterized by positive ($\nabla^2\rho_{BCP}$) values (ranging from 0.0266 to 0.2164) showing that they may be classified as ionic interactions. However, in Be^{2+} complexes, the corresponding H_{BCP} values are negative (ranging from −0.0085 to −0.0102), which means these interactions are at least partly covalent. The values of ρ at the BCPs decrease as one goes from Li^+ to Na^+ then to K^+ complexes (Table 1). The value of ρ at the BCP reflects the strength of cation–π interaction, with low values corresponding to weak interactions, and the ρ value increases as

the strength of interaction increases. Also, the trend of reduction in ρ values on going from Be^{2+} to Mg^{2+} is in agreement with the decrease of the strength of cation–π interaction (Table 1). It should be noted that the values of the Laplacian also decrease as the atomic size of the cation increases (Table 1). The similar results were reported by Dinadayalane et al. [15, 16] in the case of cation–π interactions of alkali-metal ions with the ligands benzene, naphthalene, phenanthrene, triphenylene, bicyclo[2.1.1] hexenobenzene, bis (bicyclo[2.1.1]hexeno) benzene, and tris(bicyclo[2.1.1]hexeno)benzene. Figure 2 presents molecular graph of three complexes analyzed in this manuscript. As shown in this Figure, there are two noticeable kinds of the bond paths formed. In system A-Be^{2+}, BPs corresponding to the cation–π interactions are simply formed between the metal cation Be^{2+} and the carbon atoms, and the exploration of the BCPs reveals the presence of six (3, −1), six (3, +1), and one (3, +3) BCPs symmetrically distributed following the full point group of the molecule (Cs), whereas in complexes of B-Be^{2+} and G-Be^{2+}, BPs are formed between the cation Be^{2+} and the BCP of the C–C bond of the central aromatic ring and the examination of the BCPs discloses the presence of two (3, −1), two (3, +1) and one (3, +3) BCPs symmetrically distributed. On the other hands, the BCP is made between ion and each carbon atom of benzene ring in A-Li^+, A-Na^+, A-K^+, A-Be^{2+}, A-Ca^{2+}, A-Mg^{2+}, B-Li^+, B-Na^+, B-K^+, B-Ca^{2+}, C-K^+, and C-Ca^{2+} complexes. Also, the BCP is made between ion and two π-bond of benzene ring in B-Be^{2+}, B-Mg^{2+}, C-Li^+, C-Be^{2+}, C-Mg^{2+}, F-Li^+, F-Be^{2+}, F-Mg^{2+}, G-Li^+, G-Na^+, G-Be^{2+}, and G-Mg^{2+} complexes. The results presented in Table 3 indicate a linear relationship between the values of ρ_{BCP} and $\Delta E_{ion-\pi}$ with a good correlation coefficient (R is equal to 0.983). Thus, ρ_{BCP} may be a useful parameter describing the strength of ion–π interactions. Moreover, the changes of ρ at BCPs of C=C ($\rho_{C=C}$), C–R′ ($\rho_{C-R'}$), and C–H (ρ_{C-H}) bonds have been examined upon complexation. This examination (investigation) revels that in the presence of cation–π interactions, the increment in $|\Delta E_{ion-\pi}|$ is accompanied with reduction in $\rho_{C=C}$, and also the increase in $\rho_{C-R'}$ value. A reverse relationship exists between the $\rho_{C=C}$ and $\rho_{C-R'}$ values and their corresponding bond lengths. Besides, it can be stated that with the exception of B–Be^{2+} complex, cation–π interactions increase the electron density at the BCP of C–H bond (see Table 1).

The changes of electron densities of hydrogen and R′ atoms (ρ_H and $\rho_{R'}$) have also been considered upon complexation (see Table 1). These values are related to the electron density at the nuclear critical points. Our theoretical results confirm that the interaction between cations and π electrons reduces the ρ_H and $\rho_{R'}$ values. Different features of the electron densities analysis obtained in the

Table 2 Calculated aromaticity indices, stretching frequencies (v, in cm^{-1}) of ion–π, the total electron energy densities and its components at the critical point (in a.u.), values of the quadrupole moment (in B) and dipole moment (in Deby)

Complex	HOMA	FLU	FLUπ	PDI	NICS(1)	v	δout	H	G	V	Q_{ZZ}	μ (D)
A-Li$^+$	0.9968	0.00005	0.0009	0.4086	−10.7336	382.57	755.27	0.0043	0.0184	−0.0142	−27.34	4.76
A-Na$^+$	0.9983	0.0002	0.0012	0.4145	−9.8012	191.35	737.08	0.0026	0.0096	−0.0070	−31.79	6.24
A-K$^+$	0.9994	0.00002	0.0004	0.4016	−10.1105	128.14	725.17	0.0017	0.0063	−0.0047	−38.55	6.89
A-Be^{2+}	0.9490	0.00003	0.0003	0.3902	−9.2894	598.92	843.59	−0.0090	0.0531	−0.0616	−16.74	4.00
A-Mg^{2+}	0.9685	0.0001	0.0002	0.4334	−8.6443	354.40	798.91	0.0026	0.0251	−0.0225	−24.41	7.30
A-Ca^{2+}	0.9890	0.0002	0.0001	0.3642	−10.2750	267.31	780.10	0.0012	0.0172	−0.0160	−31.36	8.57
B-Li$^+$	0.9994	0.0013	0.0006	0.3722	−10.1709	353.14	892.59	0.0038	0.0161	−0.0123	−47.22	5.36
B-Na$^+$	0.9995	0.0011	0.0004	0.3777	−9.6968	180.86	878.44	0.0023	0.0081	−0.0058	−52.07	7.33
B-K$^+$	0.9988	0.0013	0.0004	0.3695	−9.9723	96.80	867.97	0.0015	0.0052	−0.0037	−43.89	8.40
B-Be^{2+}	0.9514	0.0040	0.0020	0.3455	−8.8735	658.02	944.42	−0.0090	0.0519	−0.0609	−33.42	4.68
B-Mg^{2+}	0.9739	0.0038	0.0019	0.3874	−8.0712	342.86	915.66	0.0022	0.0234	−0.0213	−42.14	8.95
B-Ca^{2+}	0.9940	0.0030	0.0014	0.3249	−9.9459	261.24	899.26	0.0012	0.0158	−0.0146	−37.15	10.55
C-Li$^+$	0.9968	0.0013	0.0004	0.3647	−9.6090	362.19	880.22	0.0040	0.0170	−0.0131	−52.98	5.21
C-Na$^+$	0.9991	0.0012	0.0003	0.3718	−8.9313	177.21	863.57	0.0024	0.0085	−0.0061	−59.58	7.36
C-K$^+$	0.9999	0.0008	0.0004	0.3662	−9.3018	123.23	848.26	0.0015	0.0056	−0.0040	−67.91	8.64
C-Be^{2+}	0.9226	0.0037	0.0018	0.3271	−7.7606	625.69	932.04	−0.0100	0.0557	−0.0653	−27.63	4.58
C-Mg^{2+}	0.9548	0.0040	0.0020	0.3703	−6.8910	352.73	904.29	0.0024	0.0257	−0.0233	−40.16	9.13
C-Ca^{2+}	0.9850	0.0028	0.0013	0.3136	−8.8952	271.09	886.46	0.0012	0.0174	−0.0161	−53.93	10.71
D-Li$^+$	0.9939	0.0030	0.0017	0.3530	−9.3512	387.72	876.12	0.0043	0.0191	−0.0148	−36.68	4.44
D-Na$^+$	0.9971	0.0021	0.0014	0.3610	−8.8261	198.69	862.54	0.0026	0.0098	−0.0072	−31.87	6.07
D-K$^+$	0.9989	0.1523	0.1508	0.3514	−9.2381	111.30	848.02	0.0017	0.0066	−0.0050	−46.79	6.86
D-Be^{2+}	0.9106	0.0083	0.0055	0.3300	−7.5255	649.25	929.68	−0.0100	0.0585	−0.0682	−37.18	4.11
D-Mg^{2+}	0.9439	0.0069	0.0043	0.3683	−6.7414	359.90	898.03	0.0024	0.0273	−0.0249	−25.84	7.60
D-Ca^{2+}	0.9786	0.0069	0.0044	0.3022	−9.0218	281.77	885.62	0.0012	0.0189	−0.0177	−40.18	8.80
E-Li$^+$	0.9883	0.0571	0.0643	0.3763	−8.1776	386.17	857.52	0.0043	0.0191	−0.0148	−54.04	4.70
E-Na$^+$	0.9932	0.0015	0.0007	0.3564	−7.9718	196.94	842.22	0.0027	0.0099	−0.0073	−49.07	6.57
E-K$^+$	0.9961	0.0019	0.0008	0.3492	−8.2986	136.70	827.24	0.0017	0.0066	−0.0049	−60.65	7.53
E-Be^{2+}	0.8866	0.0617	0.0674	0.3392	−5.4914	607.84	913.40	−0.0100	0.0610	−0.0711	−53.38	4.37
E-Mg^{2+}	0.9271	0.0048	0.0028	0.3468	−5.0768	364.19	881.61	0.0025	0.0285	−0.0260	−41.35	8.39
E-Ca^{2+}	0.9689	0.0043	0.0024	0.2890	−7.3389	290.27	864.24	0.0012	0.0193	−0.0181	−53.82	9.30
F-Li$^+$	0.9910	0.1023	0.1173	0.4600	−9.6054	404.81	853.44	0.0046	0.0204	−0.0159	−38.94	4.46
F–Na$^+$	0.9942	0.0007	0.0003	0.3884	−8.9881	208.62	839.61	0.0028	0.0107	−0.0079	−45.71	6.30
F-K$^+$	0.9963	0.0007	0.0002	0.3770	−9.6620	115.82	828.20	0.0018	0.0071	−0.0054	−52.43	7.20
F-Be^{2+}	0.9183	0.1132	0.1286	0.4272	−8.5182	622.37	902.93	−0.0090	0.0592	−0.0686	−39.38	3.65
F-Mg^{2+}	0.9444	0.0548	0.0619	0.3958	−7.8217	371.23	874.25	0.0029	0.0286	−0.0258	−28.17	7.44
F-Ca^{2+}	0.9768	0.0017	0.0005	0.3327	−9.5244	287.76	862.21	0.0011	0.0195	−0.0184	−45.28	9.08
G-Li$^+$	0.9837	0.1066	0.1196	0.4063	−8.0705	404.11	865.66	0.0046	0.0209	−0.0163	−40.49	2.98
G-Na$^+$	0.9903	0.1031	0.1233	0.4150	−7.6318	211.06	855.13	0.0029	0.0110	−0.0081	−35.44	4.58
G-K$^+$	0.9941	0.0037	0.0021	0.3395	−8.2013	114.42	845.51	0.0019	0.0077	−0.0058	−48.21	5.27
G-Be^{2+}	0.8602	0.0718	0.0755	0.3660	−5.5590	638.73	911.47	−0.0100	0.0642	−0.0743	−39.97	3.39
G-Mg^{2+}	0.9070	0.1122	0.1233	0.4252	−4.2010	369.96	879.30	0.0026	0.0303	−0.0277	−29.10	6.44
G-Ca^{2+}	0.9591	0.0085	0.0058	0.2829	−7.4693	297.10	871.98	0.0011	0.0212	−0.0201	−41.29	7.45

AIM framework. For illustration, the contour maps of Laplacian of electron density ($\nabla^2\rho$) for the A-Be^{2+}, B-Be^{2+}, and G-Be^{2+} complexes are shown in Fig. 3. The cation–π interactions can be characterized in terms of the

properties of the Laplacian of the electron density. The sign of the Laplacian is determined by the positive curvature of ρ_{BCP} along the interaction line, as the Pauli Exclusion Principle leads to a relative depletion of charge density in

Table 3 Correlation matrices for the correlation among aromaticity indices, BCP properties, and NMR data for benzene and its derivatives

Index	HOMA	FLU	FLUπ	PDI	$\Delta E_{\text{ion}-\pi}$	NICS(1)	$\rho_{\text{(BCP)}}$	$\nabla^2\rho_{\text{(BCP)}}$	G	H	$d_{\text{ion}-\pi}$	υ	$\Delta E_{\text{(H-L)}}$	δ^H	$^1J_{\text{C-C}}$	$^1J_{\text{C-H}}$	$^1J_{\text{C-R'}}$
HOMA	1																
FLU	0.290	1															
FLUπ	0.284	**0.997**	1														
PDI	0.075	0.403	0.441	1													
$\Delta E_{\text{ion}-\pi}$	**0.926**	0.191	0.187	0.094	1												
NICS(1)	0.772	0.332	0.325	0.079	0.548	1											
$\rho_{\text{(BCP)}}$	0.880	0.169	0.166	0.115	**0.983**	0.465	1										
$\nabla^2\rho_{\text{(BCP)}}$	0.893	0.248	0.369	0.044	**0.956**	0.525	0.969	1									
G	0.889	0.214	0.213	0.210	**0.974**	0.485	0.994	0.986	1								
H	0.735	0.077	0.069	0.214	0.865	0.284	0.899	0.782	0.876	1							
$d_{\text{ion}-\pi}$	0.709	0.210	0.222	0.133	0.803	0.366	0.856	0.932	0.890	0.621	1						
υ	0.774	0.201	0.207	0.026	0.882	0.385	**0.933**	0.971	0.952	0.743	**0.974**	1					
$\Delta E_{\text{(H-L)}}$	0.569	0.272	0.270	0.255	0.347	0.017	0.251	0.304	0.248	0.042	0.151	0.158	1				
δ^H	0.387	0.223	0.215	0.122	0.588	0.115	0.570	0.540	0.534	0.427	0.503	0.519	0.037	1			
$^1J_{\text{C-C}}$	0.580	0.123	0.136	0.143	0.670	0.115	0.634	0.663	0.633	0.443	0.597	0.606	0.165	0.618	1		
$^1J_{\text{C-H}}$	0.684	0.087	0.088	0.090	0.847	0.115	0.867	0.826	0.844	0.755	0.758	0.810	0.156	0.824	0.520	1	
$^1J_{\text{C-R'}}$	0.086	0.133	0.142	0.248	0.071	0.115	0.017	0.059	0.035	0.039	0.020	0.006	0.068	0.026	0.625	0.183	1

The bolded values correspond to correlation coefficients >0.9

the interatomic surface. The studied interactions are dominated by the contraction of charge density away from interatomic surface toward each of interacting species. The spatial display of Laplacian of electron densities ($\nabla^2\rho$) is confined separately to each interacting species, reflecting the closed-shell interaction. Among all complexes, the obtained values of the electron density are the least for the interaction of the K^+ ion with the substituted benzene, while this interaction for the Be^{2+} ion creates the greatest electron density at the BCP along the interaction line. A common feature of cation–benzene interaction is the formation of a cage critical point[(CCP, ρ (3, +3)] along the line connecting the cation to the center of the ring upon complexation. It has been demonstrated that the electron density at the cage critical point can be used as a measure of the binding strength [39]. The correlation between interaction energies of cation–benzene complexes and their electron density at the CCP shows the regression coefficient of 0.916. Moreover, their obtained values permit us to have a better understanding of these novel correlations. The derived relationships from these correlations also empower us to acquire other physically meaningful results.

Charge transfer (NBO analysis)

The NBO analysis of the studied complexes is carried out to assess the charge transferred and orbital interactions established, and the results are presented in Table 4. One can see that the most important donor–acceptor interaction in the analyzed complexes is $\pi_{\text{C-C}} \rightarrow \text{Lp}^*_{\text{cation}}$ interaction. In the studied complexes, $\pi_{\text{C-C}}$ of the benzene ring participates as donor and $\text{Lp}^*_{\text{cation}}$ acts as acceptor. Calculated interaction energies, $E^{(2)}$, at UB3LYP/6-311++G** level lie in the range of 0.5–51.12 kcal mol^{-1}. In all of the substituted benzene rings, the minimum and maximum values of $E^{(2)}$ correspond to the K^+ and Be^{2+} ions, respectively. In some cases, the stronger interaction is accompanied with decreasing occupation number of $\pi_{\text{C-C}}$. Results of theoretical calculations on the Be^{2+} complexes show that upon substitution the $E^{(2)}$ values increase, which confirm that the cation–π interactions are stronger in the substituted complexes. As it is obvious from Table 4, the electron-withdrawing substituents reduce the ability of the $\pi_{\text{C-C}}$ to donate electron density into the $\text{Lp}^*_{\text{cation}}$ orbital, and hence decrease the $E^{(2)}$ values and weaken the cation–π interaction, while this is vice versa for the electron-donating substituents (except for CH_3). Therefore, our theoretical results show that the trend in the energies of these interactions ($E^{(2)}$) is identical with $|\Delta E_{\text{ion}-\pi}|$ and ρ_{BCP} parameters (Tables 1 and 4). The obtained data also demonstrate that the charge transfer for alkaline-earth metal complexes is more considerable than that for alkali-metal
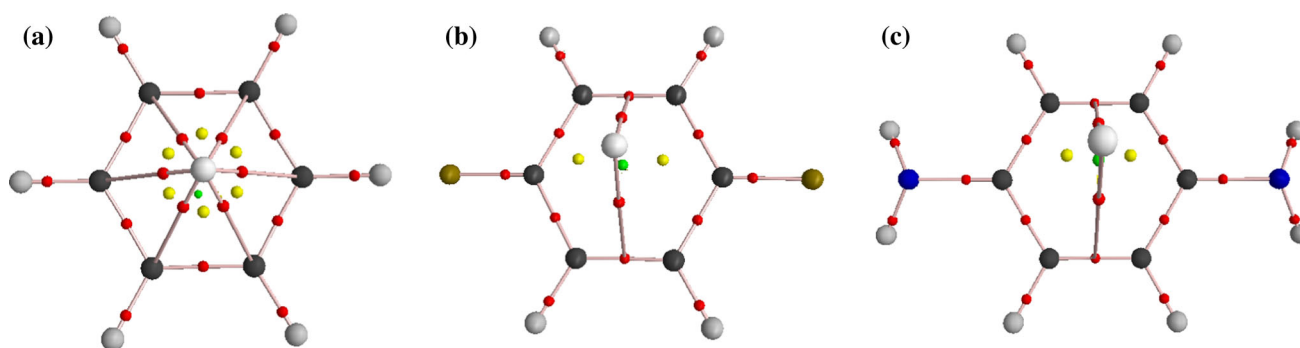
Fig. 2 Schematic representation of distribution of critical points in **a** A-Be^{2+}, **b** B-Be^{2+}, and **c** G-Be^{2+} complexes. Small *red spheres*, small *yellow spheres*, small *green sphere* and *lines* represent bond

critical points (BCPs), ring critical points (RCPs), cage critical point (CCP), and bond paths, respectively (Color figure online)

complexes (Table 4). The obtained consequences from the compared Li$^+$, Na$^+$, and K$^+$ cations ensure that the charge transfer from the π_{C-C} of the benzene ring to Li$^+$ cation is the greatest. This result can be supported by less charge on the Li$^+$ cation with respect to Na$^+$ and K$^+$ cations in the related complexes. A positive charge on the Li$^+$, Na$^+$, and K$^+$ cations in the NH$_2$-substituted complexes (0.459 |e|, 0.758 |e|, and 0.976 |e|, respectively) demonstrates that these complexes transfers the smaller amounts of charge to the Na$^+$ and K$^+$ than to Li$^+$ cation. Also, it can be seen that among the divalent metal cations, the greatest charge transfer occurs in the G-Be^{2+} complexes (0.584 |e|), while the smallest ones belong to the G-Ca^{2+} complexes (1.393 |e|). Therefore, the charge decrease on the metal cations is found to be in the order Be^{2+} > Mg^{2+} > Ca^{2+} for the corresponding alkaline–earth metal complexes. Furthermore, the results of the electron transfer in the studied complexes show that the atomic charges of cations in complexes are smaller than the isolated cations. The charge transfers (Δq_{CT}) for the investigated complexes are listed in Table 4. The amount of charge transfer between the substituted benzene rings and a cation is easily determined as the difference between the charge of the isolated cation and the atomic charge of the metal cation in the corresponding complexes. It can be seen from Table 4, clearly, the greatest charge transfer occurs in the Be^{2+} complexes, while the smallest of that belongs to the K$^+$ complexes. Besides, the smaller radius and the more electron density of the metal ion are accompanied with the more charge transfer from the benzene ring to the metal ion.

It is worth mentioning that NBO energy connected to $E^{(2)}$ $\pi_{C-C} \rightarrow Lp^*_{cation}$ overlap nicely correlates with the other geometrical and topological parameters. For example, there is a good correlation between $E^{(2)}$ $\pi_{C-C} \rightarrow Lp^*_{cation}$ versus $d_{ion-\pi}$, $\Delta E_{ion-\pi}$, and ρ_{BCP}; The correlation coefficients are equal to 0.786, 0.931, and 0.928, respectively. This implies that the properties of the charge transfer between the π_{C-C}

and Lp^*_{cation} can be very useful to estimate the strength of the cation–π interactions. The NBO analysis also describes the bonding in terms of the natural hybrid orbitals. The atomic charge distribution and percentage of the s-character of π_{C-C} and the p-character of Be^{2+} and K$^+$ cations in the G-Be^{2+} and G-K$^+$ complexes are also investigated. The p-character of Be^{2+} cation natural hybrid orbitals of $Lp^*_{Be^{2+}}$ in G-Be^{2+} complex (sp$^{9.64}$) is larger than the p-character of $Lp^*_{K^+}$ in G-K$^+$ complex (sp$^{0.69}$), similarly, the $d_{ion-\pi}$ distance in G-Be^{2+} complex (1.351 Å) is also shorter than the usual $d_{ion-\pi}$ distance in G-K$^+$ complex (2.813 Å). Our theoretical results show that the $d_{ion-\pi}$ is essentially controlled by the p-character of these hybrid orbitals. Furthermore, in comparison with the G-Be^{2+} complex (0.96 %), the reduction of the s-character of the π bonding orbitals of C–C benzene in the G-K$^+$ complex (0.07 %) is accompanied with the decrease in the complex formation energy. Figure 4 displays the 3D NBO contour plot illustrating the interaction between the π bonding orbitals of C–C benzene with an antibonding lone pair of Be in H-Be$^+$, NH$_2$-Be$^+$, and F-Be$^+$ complexes.

NMR analysis

Table 5 presents some NMR data calculated at UB3LYP/6-311++G** level of theory.

As it can be seen from this Table, the maximum and minimum of isotropic value of the proton shielding tensor corresponds to the K$^+$ and Be^{2+}complexes, respectively (except for E–Be^{2+}and G–Be^{2+} complexes). This trend is reversed for the isotropic chemical shift of H atom (δ^H). The substituents can also affect on isotropic value of the proton shielding tensor in the above-mentioned complexes. For all of substitutions, in comparison with the corresponding values of unsubstituted complexes, the isotropic value of the proton shielding tensor has been increased, while the isotropic chemical shift of H atom (δ^H) has been decreased. The meaningful relationships can be observed between the calculated NMR data and the geometrical

Fig. 3 The contour map representing **a** A-Be^{2+}, **b** B-Be^{2+}, and **c** G-Be^{2+} complexes

parameters (see Tables 5, 1). As can be seen in Table 5, the cation–π interaction decreases the isotropic value of proton and R′ shielding tensors (H and R′ shieldings) so that the maximum |$\Delta E_{ion-\pi}$| value corresponds to the minimum H and R′ shieldings (except for E-Be^{2+}and G-Be^{2+} complexes due to H shielding). As it is obvious from Tables 1 and 5, the reduction of H and R′ shielding is associated with the increase in the positive charge on the H atom and the decrease in the absolute values of negative charge on the R′ atom (except for F-Be^{2+}).

Calculated hydrogen chemical shifts of the studied complexes (δ^H) are gathered in Table 5. From this Table, the increase in the value of the H shielding tensor is accompanied with the decrease in the chemical shift of this atom. The relationship between the H (and R′) shielding and the ion–π distance is reversed when the H (and R′) shielding is replaced by the chemical shifts. In this work similar to earlier studies, a downfield shift of ^{1}H nmr spectra of the ligands is observed by interactions of metal ions.

Herein, the substituent effect on the spin–spin coupling constant $^1J_{C-C}$, $^1J_{C-R'}$ and $^1J_{C-H}$ has been investigated (see Table 5). Most coupling constants (J) have positive values. With regard to Table 5, the values of $^1J_{C-C}$ increase by both electron-donating and electron-withdrawing substituents. In comparison with $^1J_{C-C}$, the substituent effect is reversed for $^1J_{C-H}$ (except for B and C complexes) and $^1J_{C-R'}$. Furthermore, the relationship among $^1J_{C-C}$, $^1J_{C-R'}$ and $^1J_{C-H}$ coupling constants and their corresponding bond lengths has been investigated on the ion–π complexation. In the analyzed complexes, the increase in $d_{C=C}$ value is observed in the presence of cation–π interactions so that the shortest/longest $d_{C=C}$ corresponds to K$^+$/Be^{2+} complexes. In the cation–π interactions, the decrease in the value of the $^1J_{C-C}$ is accompanied with a stretch of the C–C bond. As can be seen in Table 5, the minimum and maximum values of $^1J_{C-C}$ correspond to the Be^{2+} and K$^+$ ions, respectively.

The influence of ion–π interactions on $^1J_{C-R'}$ has also been investigated in the present work. The C–R′ bond length decreases by the cation–π interactions (except for the A complexes). The shortest/longest C–R′ bond length is observed when benzene ring interacts with the Be^{2+}/K$^+$ ion. Similar to the $^1J_{C-C}$ trend, the increase in $d_{C-R'}$ is associated with the decrease in the absolute value of the $^1J_{C-R'}$ (except for the F complexes). Thus, the change of $d_{C-R'}$ value in the presence of ion–π interactions strongly affects the $^1J_{C-R'}$ value.

The $^1J_{C-H}$ is also affected by ion–π interactions. The cation–π interactions increase the $^1J_{C-H}$ value. The minimum and maximum values of the $^1J_{C-H}$ correspond to the K$^+$ and Be^{2+} ions, respectively. Moreover, the changes of d_{C-H} have been considered upon complexation. The C–H bond length increases on the cation–π interaction. A meaningful relationship is observed between the C–H bond length and the $^1J_{C-H}$ value; in this case, $^1J_{C-H}$ enriches with the increase in the C–H bond length. Among spin–spin coupling constants, $^1J_{C-H}$ shows the best linear relationship with $\Delta E_{ion-\pi}$, ρ_{BCP}, $\nabla^2\rho_{BCP}$, G, υ, and δ^H properties, with correlation coefficients greater than 0.8. This implies that coupling constants are good criteria of the cation–π interactions strength.

According to our theoretical results on the Be^{2+} and K$^+$ complexes, the Fermi-contact (FC) term is the most important factor and its trend is identical to the $^1J_{C-C}$. The diamagnetic spin–orbit (DSO) term is negligible for calculating $^1J_{C-C}$. The DSO values are approximately constant and do not change with substituent. The increase in paramagnetic spin–orbit (PSO) is accompanied with the decrease in $^1J_{C-C}$ value on the cation–π complexes (except for unsubstituted complexes). The trend in spin–dipole (SD) term is also identical to the trend in $^1J_{C-C}$. All terms of $^1J_{C-R'}$ are shown that the FC term is the most important factor in this parameter ($^1J_{C-R'}$). The orders of the absolute values of FC and PSO terms are identical to that of the $^1J_{C-R'}$ values (except for the D and F complexes). The

Table 4 $E^{(2)}$ corresponds to charge transfer between $\pi_{(C-C)}$ and $LP^*_{(cation)}$ (in kcal mol^{-1}), occupation numbers (ON) and energies of mentioned orbitals and the charge transfers (Δq_{CT} in e) computed at the UB3LYP/6-311++G** level of theory

Complex	$\pi_{(C-C)} \rightarrow LP^*_{(cation)}$	ON $_{(\pi CC)}$	ON $_{LP^*(cation)}$	$E_{(\pi CC)}$	$E_{LP^*(cation)}$	Δq_{CT}
A-Li$^+$	4.12	1.6431	0.0402	−0.4533	−0.0695	0.548
A-Na$^+$	1.22	1.6558	0.0126	−0.4284	−0.0603	0.233
A-K$^+$	0.62	1.6601	0.0054	−0.4101	−0.0461	0.056
A-Be^{2+}	22.12	1.5889	0.1439	−0.7045	−0.3502	1.355
A-Mg^{2+}	12.98	1.5972	0.1134	−0.6488	−0.3564	0.979
A-Ca^{2+}	4.75	1.6273	0.0410	−0.6153	−0.2381	0.531
B-Li$^+$	3.87	1.6774	0.0358	−0.4760	−0.0822	0.484
B-Na$^+$	1.35	1.6878	0.0144	−0.4507	−0.0453	0.180
B-K$^+$	0.52	1.6912	0.0055	−0.4321	−0.0628	0.010
B-Be^{2+}	36.34	1.5607	0.2316	−0.7155	−0.3605	1.428
B-Mg^{2+}	15.20	1.6583	0.1231	−0.6703	−0.3905	0.951
B-Ca^{2+}	3.11	1.6228	0.0605	−0.6431	−0.2513	0.459
C-Li$^+$	2.88	1.6725	0.0201	−0.4672	0.0530	0.549
C-Na$^+$	1.14	1.6703	0.0119	−0.4434	−0.0654	0.251
C-K$^+$	0.52	1.6717	0.0059	−0.4265	−0.0578	0.062
C-Be^{2+}	26.08	1.6452	0.1490	−0.7006	−0.3339	1.315
C-Mg^{2+}	14.98	1.6576	0.1188	−0.6515	−0.3853	1.051
C-Ca^{2+}	3.00	1.6414	0.0579	−0.6332	−0.2606	0.617
D-Li$^+$	4.22	1.7121	0.0395	−0.4549	−0.0667	0.528
D-Na$^+$	1.90	1.7225	0.0150	−0.4318	−0.0518	0.216
D-K$^+$	0.81	1.7210	0.0063	−0.4144	−0.0640	0.017
D-Be^{2+}	32.11	1.6905	0.1650	−0.6970	−0.3286	1.433
D-Mg^{2+}	17.85	1.6997	0.1397	−0.6470	−0.3872	1.017
D-Ca^{2+}	4.07	1.6018	0.0738	−0.6071	−0.2284	0.521
E-Li$^+$	4.01	1.6962	0.0385	−0.4520	−0.0638	0.530
E-Na$^+$	1.35	1.7041	0.0129	−0.4303	−0.0284	0.223
E-K$^+$	0.50	1.6998	0.0069	−0.4153	−0.0814	0.052
E-Be^{2+}	41.24	1.6152	0.1852	−0.6708	−0.1740	1.409
E-Mg^{2+}	16.94	1.6961	0.1478	−0.6349	−0.3966	1.129
E-Ca^{2+}	5.45	1.6944	0.0591	−0.6055	−0.2993	0.576
F-Li$^+$	4.23	1.6658	0.0422	−0.4395	−0.0577	0.649
F–Na$^+$	1.23	1.6770	0.0139	−0.4166	−0.0592	0.296
F-K$^+$	0.46	0.9865	0.0031	−0.8339	0.1165	0.074
F-Be^{2+}	25.00	1.6318	0.1466	−0.6781	−0.3043	1.455
F-Mg^{2+}	14.54	1.6508	0.1167	−0.6279	−0.3548	1.205
F-Ca^{2+}	3.34	1.6124	0.0578	−0.5926	−0.2253	0.633
G-Li$^+$	3.70	1.7462	0.0234	−0.4378	0.0366	0.541
G-Na$^+$	1.97	1.7438	0.0143	−0.4156	−0.0480	0.242
G-K$^+$	0.73	1.7409	0.0072	−0.3910	−0.0188	0.024
G-Be^{2+}	51.12	1.6530	0.1979	−0.6615	−0.1561	1.416
G-Mg^{2+}	20.87	1.7348	0.1645	−0.6229	−0.3841	1.087
G-Ca^{2+}	3.13	1.6013	0.0909	−0.5872	−0.2374	0.607

value of SD is small and its sign is negative in some of cations. The DSO term is also negligible and does not change with different cations. Furthermore, the components of $^1J_{C-H}$ are listed in Table S1 (supplementary material). The orders of FC and SD terms are similar to the $^1J_{C-H}$. For the values of DSO and PSO, this trend is reversed. The SD, DSO, and PSO terms are negligible in comparison with the value of FC term.

Fig. 4 NBO contour plots illustrating the interaction between the π bonding orbitals of C–C benzene with an antibonding lone pair of Be in H-Be$^+$, NH$_2$-Be$^+$, and F-Be$^+$ complexes
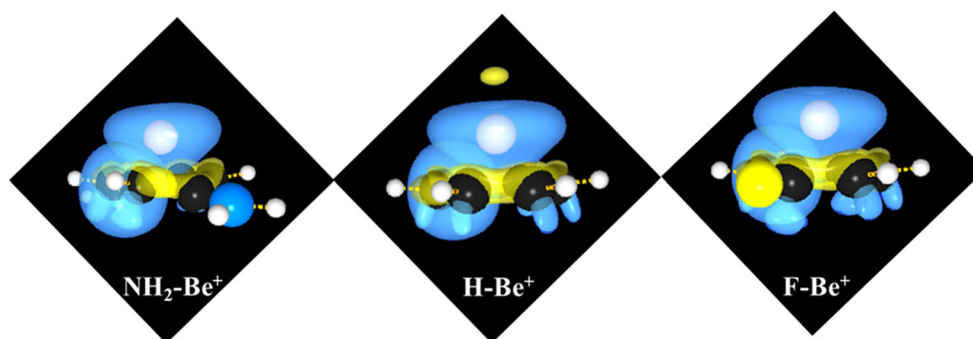
Resonance parameters

For the systems studied, the HOMA index, the NICS (1) values, the PDI, the FLU and FLUπ indicators of local aromaticity have been investigated. Table 2 shows that there is, in most cases, a good correspondence between the different indices, complexes with more negative NICS values having also larger HOMA and PDI measures and lower FLU index. As shown in Table 2, the geometry-based HOMA values are very close to the ideal aromaticity index (HOMA = 1) stated by the HOMA model and indicate that these complexes have (i) little alternation in bond lengths and (ii) average bond length values (R_{av}) near optimal (R_{opt}). Our theoretical results based on all indices, except HOMA, predict unsubstituted benzene to be more aromatic than the substituted ones, irrespective of the π-donor or -acceptor character of the substituents. The HOMA index reveals that upon F substitution, the aromaticity of benzene rings increases and the NICS values decrease with respect to the unsubstituted benzene [40]. While the HOMA values show unsubstituted complexes are less aromatic than the F-substituted ones, NICS values give an indication of higher aromaticity of these complexes. We state on the basis of these results that NICS provides an insight into benzene aromaticity, but this picture is not fully consistent with the HOMA aromaticity model [41, 42].

Regarding to NICS (1) results, upon complexation the change in aromaticity is observed. For investigated complexes, NICS (1) values are calculated below the center of the ring, on the opposite face to the ion. NICS (1) values show that the Mg^{2+} complexes have the least aromaticity, whereas the greatest aromaticity is obtained for the Li$^+$ complexes which substituted with F, Cl, OH, and CH$_3$ groups and also the K$^+$ complexes substituted with SH and NH$_2$ substitutions. As shown in Table 4, charge transfer for lithium complexes is substantially larger than for potassium complexes, so it would be expected a larger change in aromaticity for the lithium complexes. Furthermore, the results of Table 2 confirm that the aromaticity depends on the type of the substituent.

The NICS values for the electron-withdrawing substituents are more negative than the electron-donating ones (except for the F complexes). Therefore, the latter cases become less effective on the improvement of the aromaticity than the formers.

The other index to be analyzed here is the PDI descriptor of local aromaticity [37]. Due to its definition, this index can only be applied to analyze the local aromaticity of the six-membered rings of molecules. There is a satisfactory correspondence among NICS, HOMA, and PDI indices. In general, larger PDIs go with larger absolute values of NICS and larger HOMA values.

As shown in Table 2, the FLU and FLU$_\pi$ indices for the unsubstituted complexes are smaller than those for the substituted ones. Our results show that the FLU and FLUπ values are close to zero (aromatic species) and nicely correlate with together ($R = 0.997$), thus proving the similarity between FLU and FLUπ approaches. The FLUπ is found to be less correlated with the HOMA, NICS, and PDI criteria. An advantage of FLUπ with respect to FLU, apart from the fact that no reference parameters are required, is that the former gives values spread in wider ranges. For these reasons, we suggest the use of the FLUπ index for evaluation of aromaticity in planar species, since no reference systems are necessary, while the FLU index is preferred when analyzing nonplanar systems, for which an exact σ–π separation is not possible.

The correlation between different aromaticity indices and the other properties of the cation–π interactions have been checked for the investigated complexes. The correlation matrices for the correlation among aromaticity indices, $\Delta E_{ion-\pi}$, and BCP properties have been reported in Table 3. Among aromaticity indices, HOMA shows the best linear relationship with $\Delta E_{ion-\pi}$, ρ_{BCP}, $\nabla^2\rho_{BCP}$, and G properties, with correlation coefficients greater than 0.8. Whereas other indices are found to be less correlated with HOMA; however, their correlation coefficients are in acceptable range. Furthermore, $\Delta E_{ion-\pi}$ shows an excellent correlation with BCP properties (ρ_{BCP}, $\nabla^2\rho_{BCP}$, and G). This implies that the aromaticity indices can be very useful to estimate the strength of the cation–π interaction.

Table 5 Some NMR data calculated at the UB3LYP/6-311++G** level of theory

Complex	H shielding (ppm)	R′ shielding (ppm)	δ^H (ppm)	$^1J_{C-C}$ (Hz)	$^1J_{C-R'}$ (Hz)	$^1J_{C-H}$ (Hz)
A-Li$^+$	23.60	23.60	8.16	49.73	179.19	179.15
A-Na$^+$	23.71	23.71	8.05	52.26	174.24	174.25
A-K$^+$	23.86	23.86	7.90	53.73	171.57	171.60
A-Be^{2+}	22.12	22.13	9.64	39.05	210.84	211.08
A-Mg^{2+}	22.43	22.43	9.33	43.96	194.59	194.59
A-Ca^{2+}	22.69	22.69	9.07	47.03	186.41	186.40
B–Li$^+$	24.07	268.76	7.69	66.29	−352.86	183.29
B–Na$^+$	24.19	275.29	7.57	68.87	−340.88	179.04
B–K$^+$	24.34	280.13	7.42	70.45	−333.36	176.76
B-Be^{2+}	22.68	211.06	9.08	57.05	−438.71	210.71
B-Mg^{2+}	22.92	228.56	8.84	60.64	−403.94	196.98
B-Ca^{2+}	23.30	236.57	8.46	63.30	−381.27	189.89
C–Li$^+$	23.95	624.69	7.81	58.95	−40.51	184.28
C–Na$^+$	24.05	646.26	7.71	61.86	−37.85	180.34
C–K$^+$	24.17	659.31	7.59	63.62	−36.38	178.29
C-Be^{2+}	22.81	480.33	8.95	47.91	−58.72	209.82
C-Mg^{2+}	22.93	529.03	8.83	52.31	−51.41	196.21
C-Ca^{2+}	23.31	555.41	8.45	55.28	−46.18	189.56
D-Li$^+$	24.81	201.93	6.95	57.82	24.61	172.83
D-Na$^+$	24.86	207.01	6.90	60.46	24.20	168.60
D-K$^+$	24.99	210.74	6.77	62.09	23.90	166.43
D-Be^{2+}	23.63	154.62	8.13	48.91	27.92	199.19
D-Mg^{2+}	23.63	169.27	8.13	52.16	26.79	186.35
D-Ca^{2+}	24.08	177.16	7.68	54.73	25.85	179.15
E-Li$^+$	24.46	445.38	7.30	53.05	−22.55	177.74
E-Na$^+$	24.49	456.91	7.27	55.90	−20.88	173.73
E-K$^+$	24.59	464.18	7.16	57.65	−20.03	171.81
E-Be^{2+}	23.55	357.77	8.21	42.75	−33.16	202.45
E-Mg^{2+}	23.42	384.68	8.34	46.79	−29.29	189.43
E-Ca^{2+}	24.02	407.63	7.73	49.40	−25.82	182.82
F–Li$^+$	23.98	161.16	7.78	50.24	42.41	174.35
F–Na$^+$	24.06	161.32	7.70	52.93	42.72	169.67
F–K$^+$	24.26	154.01	7.39	54.53	42.99	167.22
F-Be^{2+}	22.71	156.30	9.05	39.46	37.76	203.43
F-Mg^{2+}	22.87	158.56	8.89	44.15	39.03	188.25
F-Ca^{2+}	23.16	158.97	8.60	47.24	39.65	180.17
G-Li$^+$	24.96	186.53	6.80	57.48	11.07	171.54
G-Na$^+$	24.95	187.79	6.80	59.97	9.09	167.42
G-K$^+$	25.07	188.93	6.68	61.45	8.25	165.35
G-Be^{2+}	24.19	150.12	7.56	51.63	16.28	196.28
G-Mg^{2+}	23.71	163.56	8.04	53.82	15.65	184.53
G-Ca^{2+}	24.47	168.97	7.28	55.10	12.63	177.12

Thermodynamic parameters

The thermodynamic functional changes of enthalpy (ΔH), Gibbs free energy (ΔG), and entropy (ΔS) from spectroscopic data by statistical methods are obtained at room temperature of 298.15 K and one atmospheric pressure. It

can be stated that the complexes with lower standard Gibbs energy of formation are relatively more stable, whereas those with the higher relatively standard energy of formation are more unstable. The calculated thermodynamic properties of these complexes are available in Table S2 (supplementary material). The values of the standard

enthalpies show that formation of complexes is enthalpically favored (exothermic). The values of $T\Delta S°_{298}$ implied the large entropy changes during the formation of complexes. In some cases, the high negative values of $T\Delta S°_{298}$ determine the positive values of $\Delta G°_{298}$. The formation of several systems requires the larger entropy than energy changes (in other words $|T\Delta S°_{298}| > |\Delta H°_{298}|$). In these complexes, ΔG and ΔH values are positive and negative, respectively. On the other hand, the formation of these complexes are thermodynamically disfavored ($\Delta G°_{298} > 0$), $\Delta S° < 0$ and $|\Delta H°| < |T\Delta S°|$). Therefore, the entropic factor controls the stability of these complexes. The obtained results in this study show that all of the thermodynamic properties are greatly dependent on the nature of the different cations and the R substituents. We find out that the Be^{2+}/K^{+}cations increases/decreases the stability of all complexes more than the other cations. Hence, in the most cases, the Be^{2+} complexes are characterized by the higher $\Delta G°_{298}$ value. The electronic properties of the substituents also influence the thermodynamic properties. It is worth mentioning that the SH substitution increases the stability of complexes in comparison with the other substitutions. Hence, the complexes with SH substitution are always characterized by the higher $\Delta G°_{298}$ values.

The solvent effect

In order to investigate the geometry and the complexation energy changes in the various benzene derivatives, optimization in solution is carried out using UB3LYP method with the 6-311++G** basis set. Solvation effects are accounted for using the PCM [26]. Frequency calculations indicate that the analyzed complexes have particular local minima on PES and, therefore, are stable, apart from A-Na^{+}, A-Mg^{2+}, B-Ca^{2+}, D-Na^{+}, F-Na^{+}, F-Mg^{2+}, F-Ca^{2+}, G-Na^{+}, G-K^{+}, and G-Mg^{2+} complexes that have one imaginary frequency. The calculated geometrical and topological parameters of benzene derivatives in the solution phase are available upon request as Table S3 (supplementary material). Our findings show that when the solvent effect is applied, the binding energy of complexes is significantly changed. Furthermore, the binding energy in solution is weaker than the gas phase. Our theoretical results reveal that the geometries of the studied systems do not change appreciably (except $d_{ion-\pi}$) when solvent effects are taken into account. For $d_{ion-\pi}$, an increase in distances is observed in going from the gas phase to the solution.

The PCM method predicts that the stability of the studied complexes considerably decreases in solution phase. Similar to the gas phase, the most stable systems in the solution phase are predicted to be the Be^{2+} complexes.

The difference between the binding energy of the K^{+} and Be^{2+} ions for CH_3-substituted complexes drops from -72.30 and $-1{,}045.50$ kJ mol^{-1} in the gas phase to 0.68 and -130.45 kJ mol^{-1} in the solution phase, respectively. As can be seen from Table S3 (supplementary material), the energetic preference of the Be^{2+} complexes over the K^{+} complexes in polar solvents is greater in the electron-donating groups with respect to the electron-withdrawing groups. The introduction of solvent causes the significant changes in the topological parameters and charge transfer (Δq) upon complexation, as it can be seen in Table S3 (supplementary material), the topological parameters at the BCP, such as the ρ_{BCP} and the $\nabla^2\rho_{BCP}$ of the investigated complexes in the solution phase are less than what that obtained in the gas phase. On the other hand, the cation–π interactions of the complexes in the solution phase are weaker than the gas phase. Furthermore, the charge transfer values (Δq) in the studied complexes also confirm that the interaction in solution phase is weaker than the gas phase. For instance, the charge transfers in the CH_3-substituted.

Be^{2+} complex decreases by 0.037 upon solvation

The dipole moment is the first derivative of the energy with respect to applied electric field. It is a measure of the asymmetry in the molecular charge distribution. The dipole moment of the studied systems in both the gas phase and in solvent media is reported in Tables 2 and S3 (supplementary material). In these compounds, the Ca^{2+} complexes have the largest dipole moment and the Be^{2+} complexes have the smallest ones. This may be explained by the consideration of the charge values on the metal cation. It can be mentioned that in the Ca^{2+} complexes, the Ca^{2+} cation carry the most positive charge, whereas in the Be^{2+} complexes exist the least positive charge on the Be^{2+} cation. It is noticeable that the differences between the dipole moments in these derivatives are related to nature of metal cations. In fact, high dipole moment demonstrates the high reactivity of the molecule. On the other hand, solvation is a crucial factor in the energetics and dipole moments of a wide variety of molecules. The field generated by the surrounding solvent perturbs the structures and induced a dipole moment in molecule. The neighboring solvent molecules have a large effect inducing a dipole moment more than 25 % (in water) larger than the gas phase dipole moment [43]. Since the dipole moment μ is the sum of the permanent (μ_0) and induced parts, therefore, it is expected that molecular dipole moment increases in solution. As a result of our calculations, the highest dipole moment is observed for the compounds in water solution, whereas the smallest one is belonged to the compounds in gas phase.

Fig. 5 Electrostatic potential profiles at the van der Waals surface showing the electrophilic regions (*blue*, *deepest blue* region has the most positive potential that indicates the position of the cations) and the nucleophilic regions (*red*, *deepest red* region has the most negative potential) (Color figure online)

A-Be^{2+}　　　　A　　　　A-K$^+$

B-Be^{2+}　　　　B　　　　B-K$^+$

G-Be^{2+}　　　　G　　　　G-K$^+$
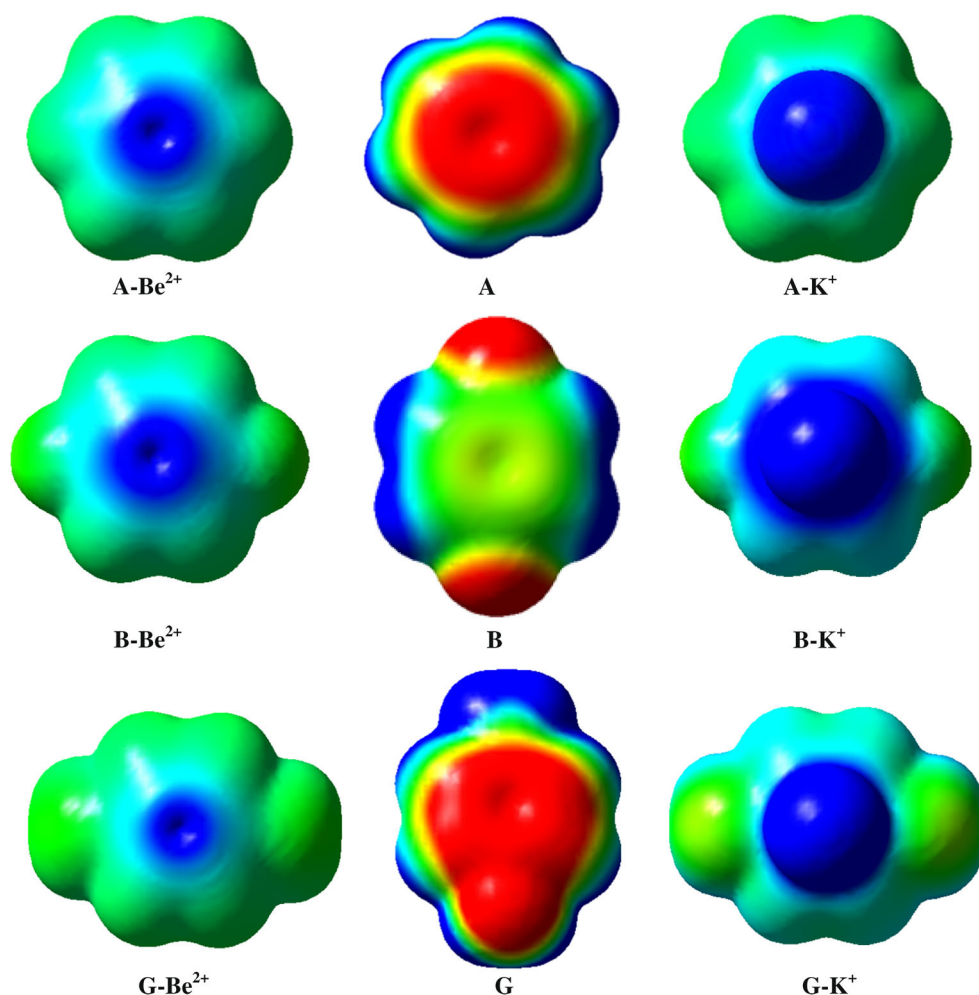
The quadrupole moment

The Garau et al. [44] showed that molecules with negligible permanent quadrupole moment values, Qzz, can interact favorably with different cations, and it is expected that the strength of the interaction would be comparable. The Benzene has substantial negative $Qzz = -8.84$ B value; 1 B (buckinghams) $= 3.336 \times 10^{-40}$ cm^2) [45]. So, this aromatic ring forms complexes only with cations, but showing large interactions energies (ranging from -33.97 to $-1,129.60$ kJ mol^{-1}). The electron-donating (or -withdrawing) effects of the substituent lead to an increase (or decrease) in the π-electron density of the aromatic ring and thereby enhance (or reduce) the quadrupole moment of the π-system. Among the investigated substitutions, both the CH$_3$ and NH$_2$ are generally referred to as electron donors because they result in an increase in the π electron density of the aromatic ring. However, the NH$_2$ substituent leads to a much greater enhancement in the π electron density than does the CH$_3$ substituent because the lone pair of electrons

on the N atom is delocalized over the aromatic ring. Such delocalization is not possible for the CH$_3$ substituent. In contrast, the F substituent is considered as an electron-withdrawing group and decreases the electron density of the aromatic π system, localizing more electron density in the plane of the aromatic ring. Thus, the values of quadrupole moments in these complexes can be arranged, respectively as: F < CH$_3$ < NH$_2$. Therefore, it can be stated that the strength of the cation–π interaction should also follow this order. The cation–π interaction between an alkali-metal ion and an aromatic ring is expected to be largely electrostatic, arising from ion–dipole, ion–quadrupole, and ion-induced dipole, but dominated by the ion–quadrupole interaction. All of these effects act in concert to increase the strength of the cation–π interaction in the CH$_3$ and NH$_2$ complexes. The effect is larger for NH$_2$ than CH$_3$ complexes, because NH$_2$ has a larger dipole moment that is oriented out of the plane of the ring and enhances the π electron density of the aromatic ring and thus the quadrupole moment to a much greater extent. In contrast, the

smaller quadrupole moment and polarizability of F substitution should weaken the binding to these complexes. In this case, the large dipole moment of the F-substituted benzene is incapable of effectively interacting with the alkali-metal ion because it lies in the plane of the aromatic ring. Furthermore, a regular trend is not observed for the quadrupole moment (Qzz) values in the studied complexes (see Table 2). As it can be seen from this Table, the quadrupole moment for these complexes is found to decrease as the size of the alkali-metal cation increases from Na^+ to K^+ (except for B complexes). Similar results have been obtained for alkaline-earth metal cations (from Mg^{2+} to Ca^{2+}).

Molecular electrostatic potential

In the present study, MEP 3D plots of the benzene and the para-substituted (F and NH_2) derivatives with K^+ and Be^{2+} cations and its uncomplexed molecular monomers are drawn in Fig. 5. The MEP is a plot of electrostatic potential mapped onto the constant electron density surface. The different values of the electrostatic potential at the surface are represented by different colors. Potential increases in the order red < orange < yellow < green < blue. The color code of these maps is in the range from -0.01980 a.u. (deepest red) to 0.01980 a.u. (deepest blue) in compound, where blue indicates the strongest attraction and red indicates the strongest repulsion. The molecular electrostatic potential profiles of the uncomplexed molecular fragments seem to guide the site of interaction with the metal ion in the equilibrium geometry of complexes. The differences in the electrostatic potential profiles of the molecules in both their uncomplexed and complexed forms are shown in Fig. 5. Regions of negative V(r) are usually associated with the lone pair of electronegative atoms. As can be seen from the MEP map of the studied complexes, the regions having the negative potential are over the electronegative atom (Fluor atom) and the plane of the benzene ring. The three dimensional electrostatic potential profile of monomers of benzene (A) and benzene-1,4-diamine (G) indicates a complete cover of the aromatic ring with negative potential, whereas in monomer 1,4-difluorobenzene (B) the negative potential cover is partial. The aromatic ring in the complexes of benzene and para-substituted (F and NH_2) derivatives is completely devoid of negative potential (Fig. 5). The regions having the positive potential are over K^+ and Be^{2+} cations and the hydrogen atoms of the benzene ring (indicated by deepest blue color). Consequently, the position of the Be^{2+} cation is tilted closer toward the plane of the benzene ring in the equilibrium geometry of benzene complexes and its derivatives, whereas the K^+ cation remain over the aromatic ring in these complexes.

Conclusions

In the present study, we have studied the structural and electronic effects of the interaction of metal cations (Li^+, Na^+, K^+, Be^{2+}, Mg^{2+}, and Ca^{2+}) with different π-systems such as the para-substituted (F, Cl, OH, SH, CH_3, and NH_2) benzene derivatives in the gas phase and the water solution by the density functional theory UB3LYP using 6-311++G** basis set. The results obtained from DFT calculations and the topological parameters derived from the Bader theory suggest that the strongest interaction and the highest electron density at BCP are related to the Be^{2+} complexes, while the weakest interaction and the smallest electron density at the BCP correspond to the K^+ complexes. It is well known that the benzene rings interact more strongly with the smaller cations, e.g., Li^+, than do with the larger cations, e.g., K^+ and, therefore, the stronger interactions lead to the lower $d_{ion-\pi}$. The influence of substituents on interactions strength is also analyzed. Electron-withdrawing groups weaken the interaction, while electron-donating substituents strengthen the cation–π binding. Moreover, the calculated electron density properties show that these interactions have low ρ and are also characterized by positive ($\nabla^2\rho_{BCP}$) values showing that they may be classified as ionic interactions, but in the Be^{2+} complexes, the corresponding H_{BCP} values are negative, which means these interactions are at least partly covalent. Our theoretical calculations show the binding energy in the substituted benzene rings in water solution is weaker than that in the gas phase. Furthermore, chemical hardness of the Mg^{2+} complexes is greater than the other derivatives of benzene, which indicates that these complexes are more stable than the others in both the gas and solution phases.

References

1. Hunter CA, Sanders JKM (1990) The nature of π–π interactions. J Am Chem Soc 112:5525–5534
2. Hashimoto S, Ikuta S (1999) A theoretical study on the conformations, energetics, and solvation effects on the cation–π interaction between monovalent ions Li^+, Na^+, and K^+ and naphthalene molecules. J Mol Struct Theochem 468:85–94
3. Ikuta S (2000) A theoretical study on the conformations and energetics on the cation–π interaction between monovalent ions ($M^+ = Li^+$, Na^+, and K^+) and anthracene and phenanthrene molecules. J Mol Struct Theochem 530:201–207
4. Aschi M, Mazza F, Di Nola A (2002) Cation–π interactions between ammonium ion and aromatic rings: an energy decomposition study. J Mol Struct Theochem 587:177–188
5. Meyer EA, Castellano RK, Diederich F (2003) Interactions with aromatic rings in chemical and biological recognition. Angew Chem Int Ed 42:1210–1250
6. Salonen LM, Ellerman M, Diederich F (2011) Aromatic rings in chemical and biological recognition: energetics and structures. Angew Chem Int Ed 50:4808–4842
7. Schneider H-J (2009) Binding mechanisms in supramolecular catalysis. Angew Chem Int Ed 48:3924–3977

8. Burley SK, Petsko GA (1985) Aromatic-aromatic interaction: a mechanism of protein structure stabilization. Science 229:23–28

9. Bhattacharyya R, Samanta U, Chakrabarti P (2002) Aromatic-aromatic interactions in and around alpha-helices. Protein Eng 15:91–100

10. Janiak C (2000) A critical account on pi–pi stacking in metal complexes with aromatic nitrogen-containing ligands. J Chem Soc Dalton Trans 21:3885–3896

11. Dougherty DA (1996) Cation–π interactions in chemistry and biology: a new view of benzene, Phe, Tyr, and Trp. Science 271:163–168

12. Steed JW, Atwood JL (2009) Supramolecular chemistry. Wiley-VCH, Weinheim

13. Ma JC, Dougherty DA (1997) The cation−π interaction. Chem Rev 97(5):1303–1324

14. Ansorg K, Tafipolsky M, Engels B (2013) Cation–π interactions: accurate intermolecular potential from symmetry-adapted perturbation theory. J Phys Chem B 117(35):10093–10102

15. Dinadayalane TC, Afanasiev D, Leszczynski J (2008) Structures and energetics of the cation–π interactions of Li$^+$, Na$^+$, and K$^+$ with cup-shaped molecules: effect of ring addition to benzene and cavity selectivity. J Phys Chem A 112:7916–7924

16. Hassan A, Dinadayalane TC, Grabowski SJ, Leszczynski J (2013) Structural, energetic, spectroscopic and QTAIM analyses of cation–p interactions involving mono- and bi-cyclic ring fused benzene systems. Phys Chem Chem Phys 15:20839–20856

17. Raju RK, Bloom JWG, An Y, Wheeler SE (2011) Substituent effects on non-covalent interactions with aromatic rings: insights from computational chemistry. Chem Phys Chem 12(17):3116–3130

18. Hunter CA (2002) In: Proceedings of the National Academy of Sciences 99(8):4873–4876

19. Wheeler SE, Houk KN (2009) Substituent effects in cation/π interactions and electrostatic potentials above the centers of substituted benzenes are due primarily to through-space effects of the substituents. J Am Chem Soc 131(9):3126–3127

20. Vijay D, Sastry GN (2010) The cooperativity of cation–PI and PI–PI interactions. Chem Phys Lett 485:235–242

21. Reddy AS, Vijay D, Sastry GM, Sastry GN (2006) From subtle to substantial: role of metal ions on π–π interactions. J Phys Chem B 110:2479–2481

22. Reddy AS, Vijay D, Sastry GM, Sastry GN (2006) Reply to "comment on 'from subtle to substantial: role of metal ions on π−π interactions'". J Phys Chem B 110:10206–10207

23. Dinadayalane TC, Hassan A, Leszczynski J (2010) The effect of ring annelation to benzene on cation–π interactions: DFT study. J Mol Struc 976:320–323

24. Dinadayalane TC, Hassan A, Leszczynski J (2012) A theoretical study of cation–p interactions: Li$^+$, Na$^+$, K$^+$, Be^{2+}, Mg^{2+} and Ca^{2+} complexation with mono- and bi-cyclic ring-fused benzene derivatives. Theor Chem Acc 131:1131–1141

25. Frisch MJ, Trucks GW, Schlegel HB, Scuseria GE, Robb MA, Cheeseman JR, Zakrzewski VG, Montgomery JA, Stratmann JRE, Burant JC, Dapprich S, Millam JM, Daniels AD, Kudin KN, Strain MC, Farkas O, Tomasi J, Barone V, Cossi M, Cammi R, Mennucci B, Pomelli C, Adamo C, Clifford S, Ochterski J, Petersson GA, Ayala PY, Cui Q, Morokuma K, Malick DK, Rabuck AD, Raghavachari K, Foresman JB, Cioslowski J, Ortiz JV, Stefanov BB, Liu G, Liashenko A, Piskorz P, Komaromi I, Gomperts R, Martin RL, Fox DJ, Keith T, Al-Laham MA, Peng CY, Nanayakkara A, Gonzalez C, Challacombe M, Gill PMW, Johnson B, Chen W, Wong MW, Andres JL, Gonzalez C, Head-Gordon M, Replogle ES, Pople JA (2003) Gaussian 03, revision A.7. Gaussian, Inc, Pittsburgh

26. Miertus S, Tomasi J (1982) Approximate evaluations of the electrostatic free energy and internal energy changes in solution processes. Chem Phys 65:239–245

27. Boys SB, Bernardi F (1970) Calculation of small molecular interactions by… with reduced errors. Mol Phys 19:553–566

28. Bader RFW (1990) Atoms in molecules: a quantum theory. Oxford University, New York

29. Biegler König F, Schönbohm J (2002) Update of the AIM2000-program for atoms in molecules. J Comput Chem 23:1489–1494

30. Reed AE, Curtiss LA, Weinhold F (1988) Intermolecular interactions from a natural bond orbital, donor-acceptor viewpoint. Chem Rev 88:899–926

31. Glendening ED, Reed AE, Carpenter JE, Weinhold F (1992) NBO, Version 3.1, Gaussian, Inc., Pittsburgh

32. Wendt M, Weinhold F (2001) NBOView 1.0; Theoretical Chemistry Institute, University of Wisconsin, Madison

33. Pulay P, Hinton JF, Wolinski K (1993) In: Tossel JA (ed) Nuclear magnetic shieldings and molecular structure, vol 386. Kluwer, Dordrecht

34. Hehre WJ, Radom L, Schleyer PR, Pople JA (1986) Ab initio molecular orbital theory. Wiley, New York

35. Cyranski MK, Krygowski TM, Katritzky AL, Schleyer PvR (2002) To what extent can aromaticity be defined uniquely? J Org Chem 67:1333–1338

36. Krygowski TM (1993) Crystallographic studies of inter- and intramolecular interactions reflected in aromatic character of pi-electron systems. J Chem Inf Comput Sci 33:70–78

37. Poater J, Duran M, Sola M, Silvi B (2005) Theoretical evaluation of electron delocalization in aromatic molecules by means of atoms in molecules (AIM) and electron localization function (ELF) topological approaches. Chem Rev 105:3911–3947

38. Matito E, Duran M, Sola' M (2005) The aromatic fluctuation index (FLU): a new aromaticity index based on electron delocalization. J Chem Phys 122:014109–014117

39. Garura C, Frontera A, Quiñonero D, Ballester P, Costa A, Deya' PM (2003) Chem Phys Chem 4(12):1344–1348

40. Shishkin OV, Omelchennko IV, Krasovska M, Zabatyuk R, Gorb L, Leszczynski J (2006) J Mol Struct 791:158–164

41. Seal P, Chakrabarti S (2007) Is nucleus-independent chemical shift scan a reliable aromaticity index for planar heteroatomic ring systems? J Phys Chem 111:9988–9994

42. Ramsden CA (2010) The influence of aza-substitution on azole aromaticity. Tetrahedron 66:2695–2699

43. Onsager L (1936) Electric moments of molecules in liquids. J Am Chem Soc 58:1486–1493

44. Garau C, Frontera A, Quiñonero D, Ballester P, Costa A, Deya' PM (2004) Cation−π versus anion−π interactions: energetic, charge transfer, and aromatic aspects. J Phys Chem A 108:9423–9427

45. Doerksen RJ, Thakkar AJ (1999) Quadrupole and octopole moments of heteroaromatic rings. J Phys Chem A 103:10009–10014